Magnetoresistance magnetometry of (Ni80Fe20)1−xIrx wires with varying anisotropic magnetoresistance ratio

Vaz, C. A. F.; Blackburn, E.; Kläui, M.; Bland, J. A. C.; Gan, Li; Egelhoff, W. F.; Cambril, E.; Faini, G.; Wernsdorfer, W.

Published in:
Journal of Applied Physics

DOI:
10.1063/1.1540056

2003

Document Version:
Publisher's PDF, also known as Version of record

Spherical neutron spin polarimetry of anisotropic magnetic fluctuations in UO_2

E. Blackburn,[1,2,*] R. Caciuffo,[3] N. Magnani,[4] P. Santini,[4] P. J. Brown,[2] M Enderle,[2] and G. H. Lander[1]
[1]*European Commission, JRC, Institute for Transuranium Elements, Postfach 2340, Karlsruhe, D-76125 Germany*
[2]*Institut Laue-Langevin, Boîte Postale 156, F-38042 Grenoble, France*
[3]*Istituto Nazionale per la Fisica della Materia, Dipartimento di Fisica ed Ingegneria dei Materiali e del Territorio, Universitá Politecnica delle Marche, I-60131 Ancona, Italy*
[4]*Istituto Nazionale per la Fisica della Materia, Dipartimento di Fisica, Universitá di Parma, Parco Area delle Scienze 7/A, I-43100 Parma, Italy*
(Received 5 July 2005; revised manuscript received 6 September 2005; published 8 November 2005)

The anisotropy of magnetic fluctuations propagating along the symmetric directions Δ, Σ, and Γ in the ordered phase of uranium dioxide has been studied by applying the spherical neutron-spin polarimetry technique to inelastic neutron scattering. The dependence of fluctuation amplitudes and directions as a function of the quasiparticle wave vector **q** has been investigated along the main crystallographic directions. The observed behavior is discussed in relation to the spin dynamics of the 3-**k** transverse magnetic structure. The observed polarization behavior of the spin waves, and in particular the acoustic mode, is shown to be a natural consequence of the transverse 3-**k** magnetic structure.

DOI: 10.1103/PhysRevB.72.184411 PACS number(s): 75.30.Ds, 78.70.Nx

I. INTRODUCTION

Spherical neutron-spin polarimetry (SNP)[1,2] (also called three-dimensional polarization analysis) has proved to be very useful in determining complex magnetic structures,[3,4] but has not, as yet, often been associated with inelastic scattering studies. Although general expressions for the cross section and polarization of the scattered neutrons were derived in the early 1960s,[5,6] only one recent paper can be found in the literature where the results of inelastic scattering experiments with three-dimensional polarization analysis are reported.[7] Such experiments can, in principle, give a wealth of information on the interaction between electronic, spin and vibrational degrees of freedom, and have the potential to play an important role in the study of strongly correlated electron systems. Here, we give an account of the results we have obtained on uranium dioxide, UO_2, using the triple axis spectrometer IN20 at the Institut Laue-Langevin, equipped with the CRYOPAD-II device used for SNP. The results obtained give a detailed description of the anisotropy of the collective magnetic fluctuations modes propagating along the main symmetry directions in a cubic 3-**k** antiferromagnet in which quadrupolar and magnetovibrational interactions are known to be far from negligible.

The physical properties of UO_2 have been extensively investigated and references to the relevant literature can be found in Ref. 8, where the magnetic excitations within the ground state are reported as a function of temperature. Above $T_N=30.8$ K, UO_2 is a paramagnetic semiconductor with the cubic fluorite structure and a Γ_5-triplet crystal field ground state.[9] The uranium lattice is fcc, with each U ion surrounded by a cubic oxygen cage. Below T_N, type-I antiferromagnetic order is established, with $\mu_{\mathrm{ord}}=1.74\mu_B$ at $T=4.2$ K. This is lower than expected for a Γ_5 state ($\sim 2.06\mu_B$). The reduction of the magnetic moment has been attributed to a dynamical Jahn-Teller coupling of the Γ_5 ground state to a trigonal phonon mode.[10] The magnetic transition is first order and is accompanied by a small internal distortion of the oxygen sublattice.[11]

The bulk of the experimental evidence suggests, indirectly, that the magnetic structure is triple-**k**: three members of the star of $\mathbf{k}=\langle 001\rangle$ enter the Fourier sum describing the moment distribution in the lattice.[9,12] For a given magnetic Bragg reciprocal point, only one of the three members of the star of $\mathbf{k}=\langle 001\rangle$ can contribute and so diffraction cannot provide direct evidence for the triple-**k** state. For example, for the (001) reflection only $\mathbf{k}_z$ propagating along [001] will contribute. There are no *K* domains, as at all times, the 3-**k** structure assures that all components are present in the same volume, even if only one is selected at a given elastic diffraction peak. For a particular reflection, three *S* domains are possible. For the $\mathbf{k}_z$ component, the moments may point along [001] (the longitudinal case), or any two directions within the (001) plane (the transverse case). The magnetic structure is transverse, so the Fourier components $\mathbf{m}_k$ are perpendicular to the propagation vector **k**. Many neutron studies, in particular of the form factor,[11] have shown that the intensities are consistent with an incoherent addition of the contributions from the two transverse *S* domains. This has recently been verified using resonant x-ray scattering.[13] In the case of inelastic scattering the simple selection rule is not applicable for scattering away from a magnetic zone center; however, the 3-**k** nature of the magnetic structure ensures that there are no *K* domains and the contributions from different *S* domains may still be added incoherently. The overall symmetry remains cubic and the uranium sublattice becomes simple cubic with a four atom base. The point symmetry at the U site reduces to C_{3h} and the space group to $P3a$.

The effective spin-lattice coupling is particularly important in this system, and there is a marked anticrossing of the phonon and magnon dispersion curves along the $\Delta(=[00\zeta])$ direction at short wave vectors.[14] The energy wave vector dispersion relation for normal modes of magnetic fluctuations reported in Ref. 8 confirms previous observations by

Cowley and Dolling[14] and Buyers *et al.*[15] The splitting of the lowest spin-wave branch propagating along the Δ direction, due to the interaction with the transversely polarized Δ_5 acoustic phonon, was clearly observed by inelastic neutron scattering with polarization analysis.[8]

If the magnetic structure is 3-**k**, the magnetic modes along the Δ direction should belong to two spin-wave branches, degenerate at Γ. According to Ref. 16, two branches of quadrupolar excitations should also be present, giving excitations in the neutron energy distribution with intensities much smaller than those corresponding to spin-wave modes. In the observed spectrum, three modes can be distinguished at the magnetic zone center, one of which is weaker than the others. By introducing anisotropic exchange and quadrupolar interactions, the calculated dispersion curves for the two spin-wave branches can be brought into satisfactory agreement with the measured ones, with the single optical branch roughly lying between the two observed ones. However, it has so far proved impossible to account for the actual three-branch structure of the spectrum.

The results presented in this paper confirm the magnetic character of the excitations observed in UO_2, and complete the phenomenological picture by providing a detailed description of the anisotropy of the fluctuation amplitudes. This behavior is then shown to be characteristic of a (transverse) 3-**k** structure.

II. EXPERIMENTAL DETAILS

The experiment was performed on the same sample used in Ref. 8, namely a single crystal of ~ 9 cm^3 in volume, cut from a melt-growth crystal boule of depleted uranium dioxide. It proved to be single phase and close to stoichiometry, with a homogeneous mosaic spread of about 0.4 degrees.

The triple-axis spectrometer IN20 was operated in the fixed-$\mathbf{k}_f$ mode (k_f=2.662 $Å^{-1}$), with the standard polarized neutron setup, a Heusler monochromator-Heusler analyzer configuration (the Heusler alloy used was Cu_2MnAl). The sample was mounted on a minigoniometer, and accurately oriented with the $[1\bar{1}0]$ direction vertical prior to installation in the CRYOPAD-II device.

Using CRYOPAD-II it is possible to drive the polarization $\mathbf{P}_i$ of the incident neutron beam along any given direction and to analyze both the longitudinal and transverse components of $\mathbf{P}_f$, the polarization of the scattered beam. In such a way, all 16 correlation functions defining the most general expression of magnetic neutron scattering[5,6] can be measured.

A schematic layout of the polarimeter device is shown in Fig. 1. A zero-field region around the sample is obtained by using two Meissner shields, consisting of two coaxial Nb cylinders (258 and 294 mm diameter, respectively) cooled into the superconducting state inside a μ-metal box prior to installation on the spectrometer. Between the two Meissner shields, a toroidal solenoid generates a horizontal magnetic field $\mathbf{B}_a$ and a second coil, wound over a 45° segment of the solenoid, allows tangential and/or horizontal fields to vary for $\mathbf{k}_i$ and $\mathbf{k}_f$. Two rotatable dipole electromagnets (nutators) complete the device. The first nutator is used to rotate adiabatically the neutrons spins (the spin component parallel to the magnetic field $\mathbf{B}_{ni}$ is conserved along the neutron path), so that the polarization **P** at the surface of the outer Nb shield is orthogonal to the incident wave vector $\mathbf{k}_i$ and forms an angle θ_{in} to the vertical axis, defined by the nutator orientation. The passage into the annular region between the two Meissner shields is nonadiabatic, causing the polarization **P** to rotate around $\mathbf{B}_a$ by an angle χ_{in}. By choosing appropriate values for θ_{in} and for the electrical currents in the toroidal coils, the polarization of the incident beam, $\mathbf{P}_i$, can be driven to any spatial orientation. By controlling the orientation θ_{out} of the second nutator, and the precession angle χ_{out} that the beam polarization undergoes when the scattered neutrons cross the annular region, any of the three Cartesian components of the final polarization, $\mathbf{P}_f$, can be analyzed. In the following, the x axis of the reference frame is defined to be parallel to the momentum transfer $\mathbf{Q}=\mathbf{k}_i-\mathbf{k}_f$, the y axis is perpendicular to **Q** and lies in the scattering plane, and the z axis is perpendicular to the scattering plane (vertical). This means that in a given scan across reciprocal space, only the z axis remains constant in physical space.

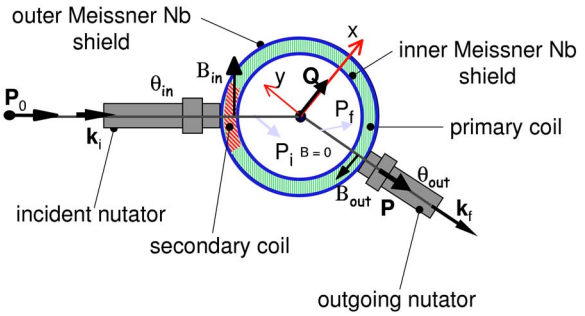

FIG. 1. (Color online) Schematic layout of CRYOPAD-II.

The generalized expression for the neutron cross section can be found in Refs. 5 and 6. One of the outcomes is that certain magneto-vibrational interference terms will rotate the neutron polarization by $\pi/2$. For example,

$$P_{fy}\sigma = (N^* M_{\perp y} + N M^*_{\perp y}) + i(N^* M_{\perp z} - N M^*_{\perp z}) P_{ix} \quad (1)$$

so that a beam initially polarized along the x direction should have a y polarization component after being scattered. In Eq. (1), σ is the double differential cross section, N indicates the vibrational scattering amplitude and $M_{\perp\alpha}$ are Cartesian components of the inelastic magnetic scattering operator. If N and $M_{\perp\alpha}$ are out of phase, the rotation is $-\pi/2$. The magneto-vibrational term, responsible for the rotation of **P**, involves correlation functions which couple the time dependences of the spin components perpendicular to **Q** and the time dependences of atomic displacements parallel to **Q** at the same position and time.

For $\mathbf{P}_i \| x$, the unrotated polarization is given by

$$P_{fx}\sigma = a + NN^* P_i - (M_{\perp y} M^*_{\perp y} + M_{\perp z} M^*_{\perp z}) P_{ix}, \quad (2)$$

where a is a polarization-independent background term. Note that we ignore the chiral magnetic term here. This means that scattering from lattice vibrations, proportional to NN^*, gives rise to a non-spin-flip (NSF) signal, whereas magnetic scat-

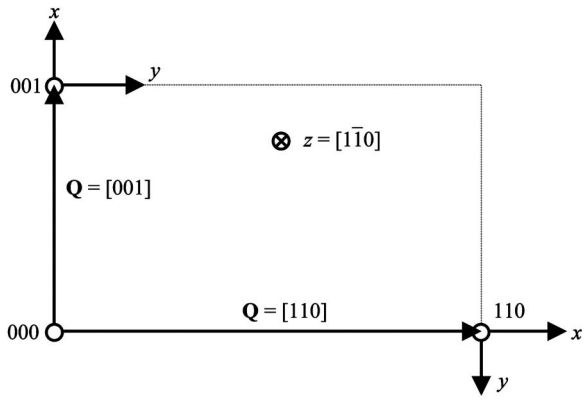

FIG. 2. The [001]-[110] scattering plane of UO_2. The x and y neutron polarization directions are shown for $\mathbf{Q}$=[001] and $\mathbf{Q}$ =[110]. The z neutron polarization direction is always parallel to [1$\bar{1}$0].

tering reverses the polarization of the beam, and hence leads to a spin-flip (SF) signal. On the other hand, with $\mathbf{P}_i \| y$ and negligible magneto-vibrational interference, one has

$$P_{fy}\sigma = NN^* P_i + (M_{\perp y}M^*_{\perp y} - M_{\perp z}M^*_{\perp z})P_{iy}. \quad (3)$$

Components of the magnetic fluctuation perpendicular to $\mathbf{Q}$ but parallel to $\mathbf{P}_i$ also give rise to NSF scattering, whereas components perpendicular to both $\mathbf{Q}$ and $\mathbf{P}_i$ produce SF scattering. P_{fz} behaves similarly.

The final polarization is extracted from SF and NSF measurements, where the SF measurement is taken with the fields in the second nutator inverted,

$$P_f = \frac{I_{\mathrm{NSF}} - I_{\mathrm{SF}} - BG_{\mathrm{NSF}} + BG_{\mathrm{SF}}}{I_{\mathrm{NSF}} + I_{\mathrm{SF}} - BG_{\mathrm{NSF}} - BG_{\mathrm{SF}}}, \quad (4)$$

where I is the integrated intensity and BG is the background.

Before starting the experiment, the CRYOPAD-II device was aligned and calibrated using the (004) Bragg reflection of a pyrolytic graphite crystal. An incident polarization P_0 =0.910(3) was obtained along three perpendicular directions. Measurements on the nuclear (002) Bragg peak of UO_2 with incident polarization parallel to z gave a scattered polarization P=0.891(1). The rotation of the neutron polarization as scattered elastically by magnetic Bragg reflections was then measured and found to be consistent with a transverse 3-$\mathbf{k}$ magnetic structure with an ⟨001⟩ propagation vector. The UO_2 crystal (99 g) was aligned with the scattering plane [001]-[110]. The neutron polarization axes x, y, and z are illustrated for two points in this scattering plane in Fig. 2.

III. RESULTS

Measurements were performed at inelastic positions spanning the whole magnetic Brillouin zone. Some example scans are shown in Fig. 3. The three panels on the left-hand side show constant-$\mathbf{Q}$ scans taken at $\mathbf{Q}$=[001]. The label α-β indicates that the initial polarization is along the α direction and that the final polarization is analyzed along the β direction. The three panels on the right-hand side show similar scans taken with the x-x, y-y, and z-z geometry at $\mathbf{Q}$ =[110]. The open and filled symbols correspond, respectively, to neutrons scattered either spin-up (NSF) or spin-down (SF) with respect to the chosen analysis direction, where the incident polarization is defined to be spin-up. A difference between these two counts implies a polarization of the scattered beam.

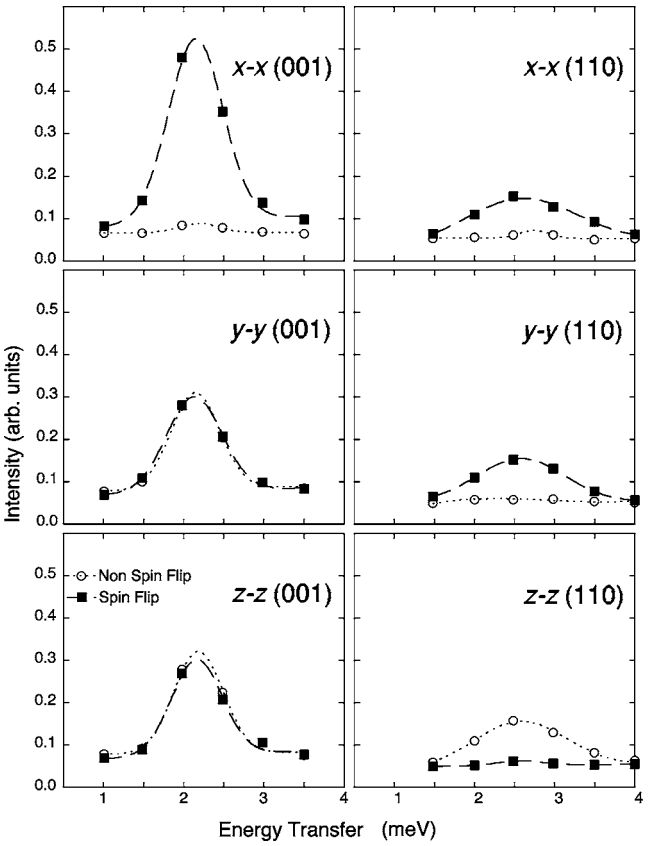

FIG. 3. Constant-$\mathbf{Q}$ scans taken at (001) (left-hand side) and (110) (right-hand side). The neutron x-x, y-y, and z-z spin-flip (SF, black squares) and non-spin-flip (NSF, open circles) cross sections are shown. The error bars are smaller than the point size.

The absence of NSF scattering in the x-x measurement indicates that the excitation centered about 2.5 meV is purely magnetic in nature. The y-y and z-z cross sections can then be used to gain further information on the polarization of the fluctuations [see Eq. (3)].

At $\mathbf{Q}$=[001], y is in the [110] direction, and z in the [1$\bar{1}$0] direction. The y-y and z-z SF and NSF signals are equal, indicating that fluctuations in the y and z directions have equal amplitudes leading to equal scattering intensity in both directions—there are isotropic fluctuations in the accessible plane. This indicates that either only one of the two transverse S domains is present, or that they are both present in equal volume (see Sec. IV). Recent x-ray resonant scattering experiments on UO_2 have found this second case to be true.[13]

At $\mathbf{Q}$=[110], y corresponds to the [001] direction. For neutron polarization in the y direction, signal appears in the SF channel only, whereas for polarization along z, it is in the NSF channel only. This indicates that there are no magnetic

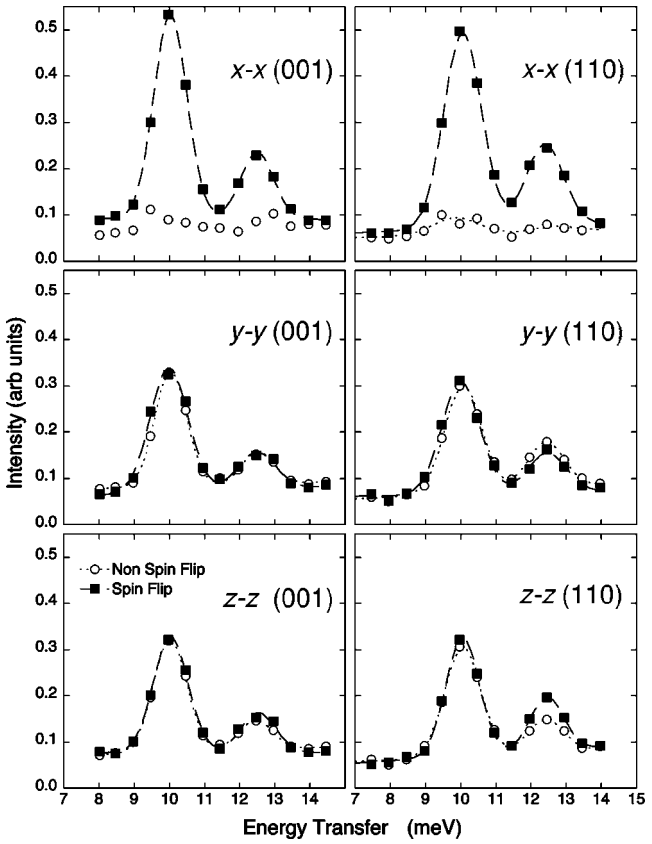

FIG. 4. Constant-**Q** scans taken at (001) (left-hand side) and (110) (right-hand side) for an energy transfer of 8–14 meV. The *x*-*x*, *y*-*y*, and *z*-*z* cross sections are shown. SF scattering is indicated by filled squares and NSF scattering by open circles. The error bars are smaller than the point size. The average counting time with full polarization analysis was 12 minutes per point.

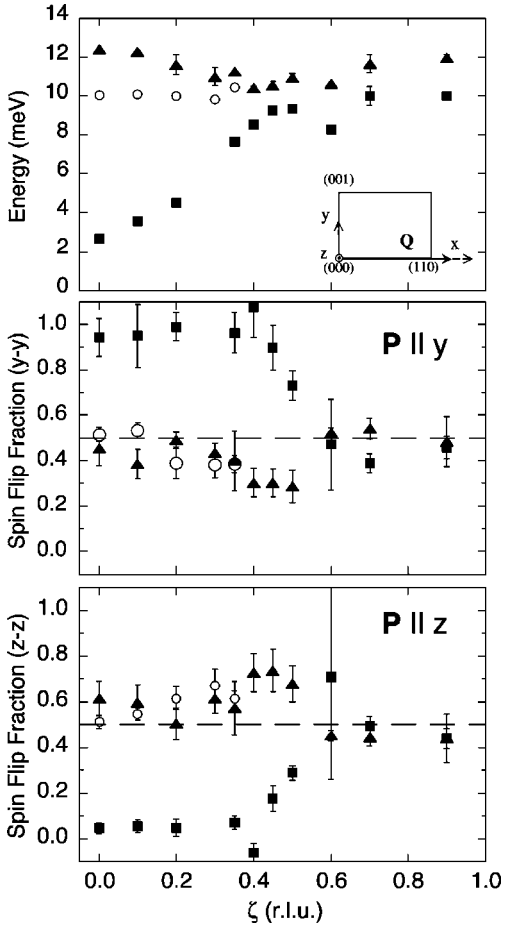

FIG. 5. The modes in the $[\zeta\zeta 0]$ direction from the 110 magnetic zone center to 220. The upper panel shows the dispersion, and the inset indicates the scattering geometry and coordinate system for the neutron polarization. The lower panels show the ratio of SF to NSF [SF/(SF+NSF)] scattering for each mode, identified by symbol type, with data taken from the *y*-*y* and *z*-*z* cross sections, respectively.

fluctuations along the [001] direction (parallel to *y*). The *z*-*z* data independently measures the same information as the *y*-*y* data. This absence of fluctuations is also responsible for the weaker intensity measured at (110), only one component of the fluctuations is visible, as compared to two in the (001) case. This leads to the intensity difference (ratio 4:1) observed at the two positions.

The above discussion focusses on the low-energy (acoustic) magnetic fluctuations. Figure 4 shows similar data taken at larger energy transfer, examining the less-dispersive magnetic modes. Again, the signal is all magnetic, but at (110) the 10 meV mode has equal amplitudes of fluctuation along *y* [001] and *z* $[1\bar{1}0]$. The (less intense) 12.5 meV mode shows a slightly larger magnetic amplitude along *y* than along *z*, evidenced by the small difference in NSF and SF scattering for the *y* direction, which is inverted with the polarization along the *z* direction. This indicates that the effect observed at low-energy transfers is a real difference and not simply due to the change in the magnetic cross section due to a shift in scattering vector. The high-energy (optic) modes correspond to isotropic magnetic fluctuations, with amplitudes of comparable size along [001], [110], and $[1\bar{1}0]$.

Information gathered from similar data sets taken at different **Q** positions was used to monitor the fluctuations of the collective modes propagating along the symmetric directions Δ, Σ, and Γ throughout the whole Brillouin zone, from the (001) and (110) reciprocal lattice points. This information is collated in Figs. 5–10. Each figure contains an inset illustrating the positioning of the scattering vector in the scattering plane. The $\mathbf{P}\|y$ and $\mathbf{P}\|z$ data sets provide two independent measurements of the same quantity, with the *z* data expected to be the mirror image of the *y* data, and this comparison emphasizes the robust nature of the data. In each case the $\mathbf{P}\|x$ data indicated that the scattering was magnetic in origin.

In Figs. 5 and 6, the behavior of the modes propagating along $[\zeta\zeta 0]$ is illustrated. The upper panels display the dispersion relation for the normal modes. In the lower panels, the vertical axis is the spin-flip fraction, defined as $I_{\mathrm{SF}}/(I_{\mathrm{SF}}+I_{\mathrm{NSF}})$ where I_{SF} (I_{NSF}) represents the integrated intensity in the spin-flip (non-spin-flip) channel. The neutron polarization geometry is as described above. The spin-flip fraction of each point in the dispersion plot can be identified by matching up the symbols.

With $\mathbf{Q}\|[110]$, magnetic fluctuations in the plane [001]-$[1\bar{1}0]$ are accessible. With incident neutrons polarized along

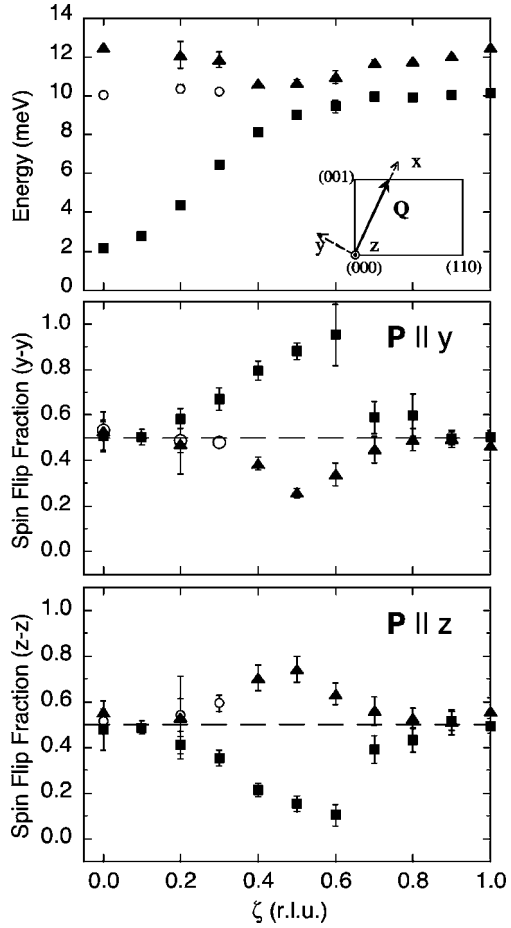

FIG. 6. The modes in the $[\zeta\zeta 0]$ direction from the 001 magnetic zone center to 111. The upper panel shows the dispersion, and the inset indicates the scattering geometry and coordinate system for the neutron polarization. The lower panels show the ratio of SF to NSF [SF/(SF+NSF)] scattering for each mode, identified by symbol type, with data taken from the *y*-*y* and *z*-*z* cross sections, respectively.

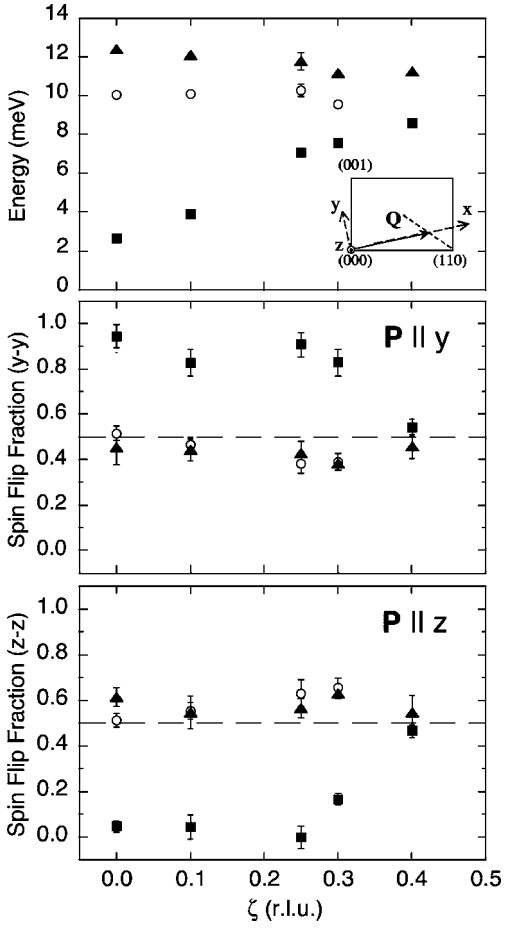

FIG. 7. The normal modes of magnetic fluctuations in the $[\overline{\zeta}\zeta\zeta]$ direction from the (110) magnetic zone center to $\frac{1}{2}\frac{1}{2}\frac{1}{2}$. The upper panel shows the dispersion relation; the inset indicates the scattering geometry and coordinate system for the neutron polarization. The lower panels show the ratio of SF to NSF [SF/(SF+NSF)] scattering for each mode, identified by symbol type, with data taken from the *y*-*y* and *z*-*z* cross sections, respectively.

y (i.e., [001]), NSF scattering is absent if fluctuations along [001] are negligible. This is observed in Fig. 5 for the dispersive mode when $\zeta<0.5$, whereas for $\zeta>0.5$ the spin-flip fraction is about 0.5, suggesting that after the branches merge, fluctuations along [001] and $[1\bar{1}0]$ have comparable magnitude. Results obtained with incident neutrons polarized along $[1\bar{1}0]$ (lower panel of Fig. 5) confirm these conclusions. Figure 6 looks at the same branches again, but this time moving away from the (001) magnetic zone center. In this geometry, fluctuations along the [110] direction are probed in place of the [001] fluctuations.

Combining the data from Figs. 5 and 6, at the magnetic zone center ($\zeta=0$) all of the modes have equal amplitude fluctutation in the $[110]$ - $[1\bar{1}0]$ plane, and the acoustic mode has no fluctuations in the [001] direction. Around the magnetic zone-boundary ($\zeta=0.5$) the excitation mode around 10 meV is polarized in the $[1\bar{1}0]$ direction, whereas the branch near 12 meV shows a small preference for fluctuations in the $[11\bar{1}]$ direction.

The modes propagating along $\langle\zeta\zeta\zeta\rangle$ are shown in Figs. 7 and 8. For small ζ values in Fig. 7, fluctuations in the [001]-$[1\bar{1}0]$ plane are explored. At low ζ, the acoustic branch is polarized along $[1\bar{1}0]$, while the nondispersive branches at higher energy are almost isotropic in the plane perpendicular to **Q**, with fluctuations along [001] and $[1\bar{1}0]$ having finite amplitude. The behavior of the acoustic branch changes on approaching the zone boundary as fluctuations in the scattering plane increase in amplitude until the mode becomes isotropic in the plane perpendicular to **Q** for $\zeta=0.5$. The plane explored in Fig. 8 remains close to [110]-$[1\bar{1}0]$; anisotropic fluctuations develop for ζ larger than about 0.25, as the three modes start to merge. Then, the mode at 10 meV (the middle branch) becomes mostly $[1\bar{1}0]$ polarized, as does the mode propagating along $[\zeta\zeta 0]$ from the (001) position. In the 12 meV mode the fluctuation amplitude along $[1\bar{1}0]$ diminishes relative to the fluctuation amplitude in the scattering plane.

In Figs. 9 and 10 the $[00\zeta]$ magnons are investigated. From the (110) point, they are investigated in transverse ge-

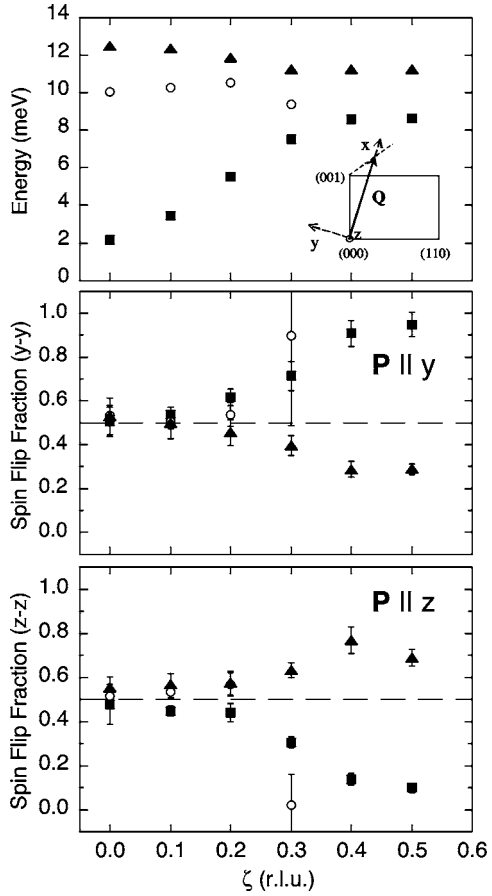

FIG. 8. The normal modes of magnetic fluctuations in the $[\zeta\zeta\zeta]$ direction from the (001) magnetic zone center to $\frac{1}{2}\frac{1}{2}\frac{3}{2}$. The upper panel shows the dispersion relation; the inset indicates the scattering geometry and coordinate system for the neutron polarization. The lower panels show the ratio of SF to NSF [SF/(SF+NSF)] scattering for each mode, identified by symbol type, with data taken from the *y*-*y* and *z*-*z* cross sections, respectively.

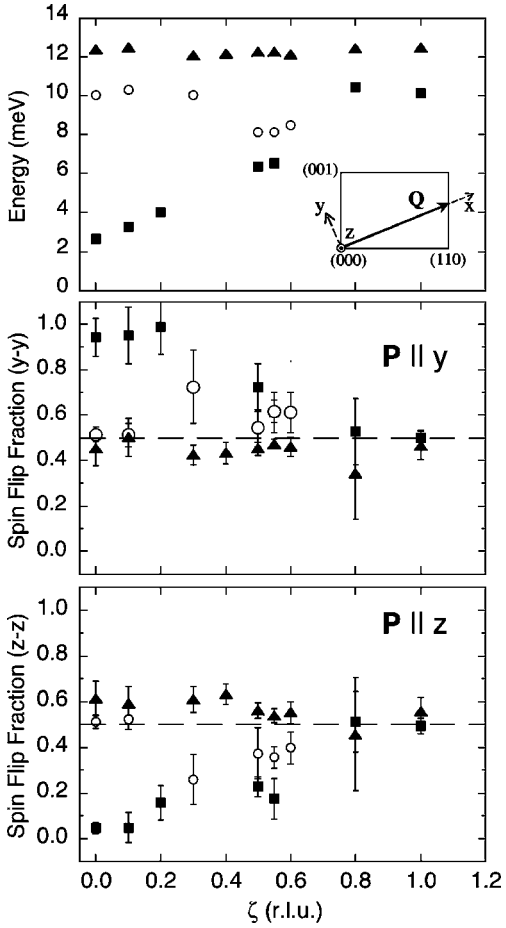

FIG. 9. The normal modes in the $[00\zeta]$ direction from the (110) magnetic zone center to 111. The upper panel shows the dispersion relation; the inset indicates the scattering geometry and coordinate system for the neutron polarization. The lower panels show the ratio of SF to NSF [SF/(SF+NSF)] scattering for each mode, identified by symbol type, with data taken from the *y*-*y* and *z*-*z* cross sections, respectively.

ometry. Close to $\mathbf{Q}=[110]$, the accessible fluctuations are in a plane close to $[001]$-$[1\bar{1}0]$. The high-energy branches are isotropic in this plane, in contrast to the behavior of the low-energy mode, which has been assumed to hybridize strongly with the transverse Δ_5 acoustic phonon. At the magnetic zone center, in fact, the $[001]$ fluctuation is not present in the lowest energy magnon branch. In longitudinal geometry (Fig. 10) the acoustic mode has equal amplitudes along $[001]$ and $[1\bar{1}0]$, like the two optic modes.

Particular attention was devoted to the region where the magnon-phonon interaction was observed.[14] In the position where the anticrossing occurs $[\sim(0\,0\,1.5)]$, a magneto-vibrational interaction should produce a $\pi/2$ rotation of the neutron spin, as outlined in Eq. (1), and cross terms of the form *x*-*y*, *x*-*z*, etc., should be observed. We looked carefully for this rotation, but none was observed (see Fig. 11). In the cross-term channels, a signal was observed at the inelastic magnetic excitation, but there was no observable difference between the spin-flip and non-spin-flip terms. From Eq. (1), this indicates that either $N^*M_{\perp z}-NM^*_{\perp z}=0$ or that there are no magneto-vibrational terms present, although the presence of polarization independent scattering indicates that there may be some, or that the in-phase and out-of-phase magneto-vibrational contributions are equal. The lack of a polarization dependent signal could also be due to the low intensity of the magnon at this point in reciprocal space, or a weak phonon cross section due to the small value of Q.

IV. MODEL AND DISCUSSION

Although spin waves in UO_2 have been experimentally investigated since the 1960s, a satisfactory theoretical understanding is still lacking. Whereas initial modeling[14] of the inelastic spectra on the basis of a 1-**k** magnetic structure was reasonably successful, it is actually much more difficult[8] to understand the spin-wave spectra on the basis of the correct 3-**k** configuration. In particular, whereas three branches are experimentally observed, two-branches are predicted by models based on dipolar exchange couplings. If quadrupolar two-ion interactions are included[16] two further branches might appear, bringing the total to four. These additional two

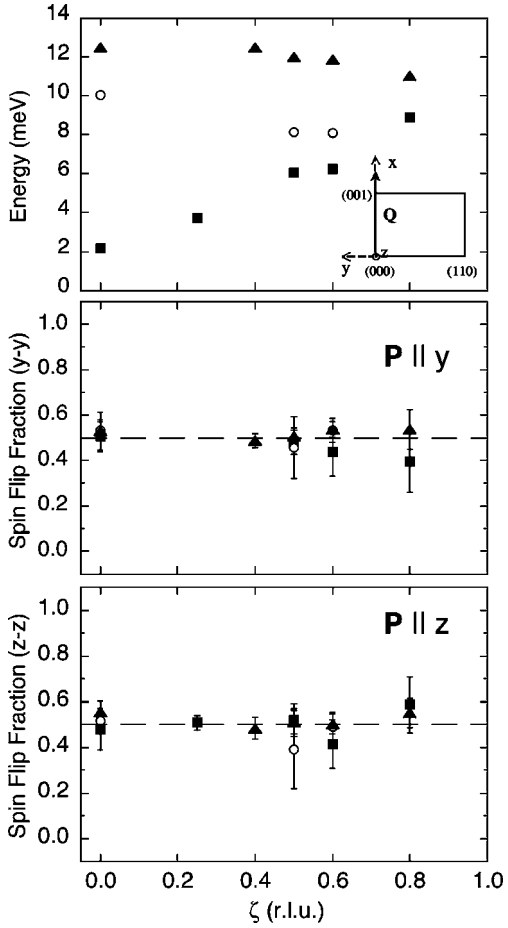

FIG. 10. The normal modes in the $[00\zeta]$ direction from the (001) magnetic zone center to 002. The upper panel shows the dispersion relation; the inset indicates the scattering geometry and coordinate system for the neutron polarization. The lower panels show the ratio of SF to NSF [SF/(SF+NSF)] scattering for each mode, identified by symbol type, with data taken from the *y-y* and *z-z* cross sections, respectively.

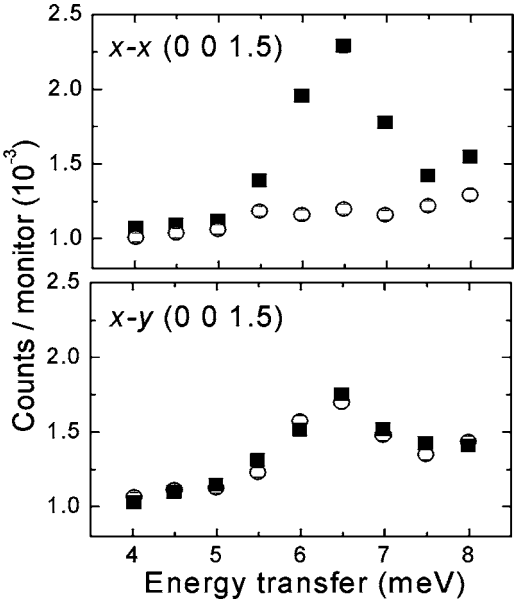

FIG. 11. Constant-**Q** scans taken at (0 0 1.5). The *x-x* (upper panel) and *x-y* (lower panel) spin-flip (black squares) and non-spin-flip (open circles) cross sections are shown. The *x-x* data illustrates the presence of magnetic signal. In the *x-y* channel, no difference is observed between the spin-flip and non-spin-flip cross sections. The error bars are smaller than the point size, and are not shown.

branches should be much weaker than the others.

In the following, for the static 3-**k** structure we use a mean-field model similar to that adopted in Ref. 16. This is based on anisotropic exchange and effective lattice-mediated quadrupolar interactions. Each U ion has an associated $S=1$ pseudospin corresponding to the Γ_5-triplet crystal-field ground state. This multiplet carries magnetic-dipole and Γ_3, Γ_5 electric-quadrupole degrees of freedom. In addition to the usual two-ion dipolar superexchange, effective quadrupole interactions are expected to arise from the magnetoelastic coupling. Excited crystal-field states lie above 150 meV and are not expected to produce qualitative changes in the low-T behavior.

Although there are four inequivalent sites, in the mean-field approximation the problem can be reduced to the study of a single self-consistent effective Hamiltonian

$$H_{\mathrm{MF}} = -JS\langle S\rangle - KQ\langle Q\rangle, \tag{5}$$

where $S=\mathbf{n}(i)\cdot\mathbf{S}(i)$ is the component of the spin along the direction of the moment $\mathbf{n}(i)$ in the ith sublattice (parallel to one of the four cube diagonals), and $Q=[(\mathbf{n}(i)\cdot\mathbf{S}(i))^2-2/3]$ is the quadrupole operator describing an axial distortion of the charge distribution along $\mathbf{n}(i)$. The first term in H_{MF} drives the order, and the second is needed to account for the first-order character of the phase transition. Since Q and S commute, the eigenstates of H_{MF} do not depend on the values of the J and K parameters, but the eigenvalues obviously do.

Spin-wave excitations are calculated within a random-phase-approximation approach.[17] This is equivalent to the method used in Ref. 16, apart from the fact that quadrupolar interactions between fluctuations are neglected. Indeed, we expect these effects to be minor,[16] the main role of quadrupolar terms in the dynamics being a modification of the single-ion energy gaps (the latter determines the overall energy scale of spin waves). The exchange is limited for simplicity to nearest-neighbor ions, and is parametrized by J and a second parameter, δ, which represents the anisotropic part of exchange.[17,18] For isotropic exchange, $\delta=0$. The stability of the transverse structure requires $\delta>0$.

The wave-vector- and frequency-dependent dynamical susceptibility tensor $\chi_{\alpha\beta}(\mathbf{Q},\omega)$, whose poles and residues correspond to the frequencies and neutron-scattering intensities of spin-wave excitations, is obtained by starting from the single-ion dynamical susceptibilities calculated with H_{MF}, and by implementing the random-phase-approximation scheme of Ref. 17. The calculation of the cross section for polarized neutrons is obtained by using the general expression[19] which describes the final polarization $\mathbf{P}_f$ of a scattered neutron beam as a function of the incident beam polarization $\mathbf{P}_i$. Defining the **x** axis as parallel to **Q** and choosing $\mathbf{P}_i \perp \mathbf{x}$ one obtains

$$P_{f\alpha}\left(\frac{d^2\sigma}{d\Omega dE}\right) \propto \{P_{iy}[S_{\alpha y}(\mathbf{Q},\omega)+S_{y\alpha}(\mathbf{Q},\omega)]+P_{iz}[S_{\alpha z}(\mathbf{Q},\omega) + S_{z\alpha}(\mathbf{Q},\omega)]-P_{i\alpha}[S_{yy}(\mathbf{Q},\omega)+S_{zz}(\mathbf{Q},\omega)]\}, \tag{6}$$

where

$$S_{\alpha\beta}(\mathbf{Q},\omega)=\frac{\chi''_{\alpha\beta}(\mathbf{Q},\omega)}{\pi[1-\exp(-\hbar\omega/k_BT)]}. \tag{7}$$

For a given $\mathbf{Q}$, $S(\mathbf{Q},\omega)$ has three poles (two of which are always degenerate), corresponding to two spin-wave branches. For the $\mathbf{Q}$ directions considered here, each diagonal term of the susceptibility tensor $\chi''_{\alpha\alpha}(\mathbf{Q},\omega)$ in the conventional cubic cell reference frame contributes a pole $\omega^{\alpha\alpha}(\mathbf{Q})$. For instance, for $\mathbf{Q}$ along [001] or [110], two of the dispersion curves $\omega^{xx}(\mathbf{Q})$, $\omega^{yy}(\mathbf{Q})$, and $\omega^{zz}(\mathbf{Q})$ are degenerate, have equal intensity, and correspond to the optical mode, whereas the third one (ω^{xx} or ω^{yy} depending on which of the two possible S domains is considered) corresponds to the acoustic branch.

As in the central panel of Figs. 5–10, we define the $\mathbf{y}$ axis as parallel to the incident-beam polarization $\mathbf{P}_i$ (we recall that the $\mathbf{x}$ axis is parallel to $\mathbf{Q}$). The $\mathbf{z}$ axis is defined by $\mathbf{x}\times\mathbf{y}$. In the following, the conventional cubic cell reference frame will be denoted by $\bar{x}$, $\bar{y}$, $\bar{z}$. For $\mathbf{P}_f\|\mathbf{y}$, the measured spin-flip fraction for a given spin-wave mode of frequency $\omega_0(\mathbf{Q})$ is given by $I_{zz}/(I_{yy}+I_{zz})$, where $I_{\alpha\alpha}=S_{\alpha\alpha}(\mathbf{Q},\omega_0(\mathbf{Q}))$, and α refers to the chosen ($\mathbf{Q}$-dependent) reference frame. For instance, by rotating the generalized susceptibility tensor to a reference frame x, y, z matching the one used in Fig. 5, one has that

$$\chi_{yy}=\chi_{\bar{z}\bar{z}};\chi_{zz}=\frac{\chi_{\bar{x}\bar{x}}+\chi_{\bar{y}\bar{y}}}{2}. \tag{8}$$

For both S domains, this leads to a y-y spin-flip fraction (central panel of Fig. 5) equal to 1 for the acoustic branch. In fact, for this branch $I_{yy}=0$ because it has no fluctuations along the cubic $\bar{z}$ axis. This is a consequence of the general behavior expected for a transverse 3-$\mathbf{k}$ structure, as discussed in the paragraphs following Eq. (7). For $\mathbf{Q}$ lying in the scattering plane [001]–[110], the eigenvalue $\omega_{\bar{z}\bar{z}}$ is associated to the optical branch, so that the acoustic branch amplitude has no contribution from $\chi_{\bar{z}\bar{z}}$. In the reference frame of the experiment (for instance the one of Fig. 5), $\chi_{yy}=\chi_{\bar{z}\bar{z}}$ is therefore zero. The spin-flip fraction is about 1/3 for the optical branch since for the latter $I_{yy}\sim 2I_{zz}$ [in fact, in the second equality of Eq. (8), only one of the two terms in the numerator is nonzero]. The corresponding z-z spin-flip fractions are simply their complements to one. This is perfectly compatible with the experimental data in the region where the acoustic and the optical branches are well separated ($\zeta \leqslant 0.5$). It should be noted that, although (as stated above) one of the two optical branches is missing in the model, experimentally these display very similar polarization properties. An example of comparison between measured and calculated inelastic neutron scattering spectra is shown in Fig. 12.

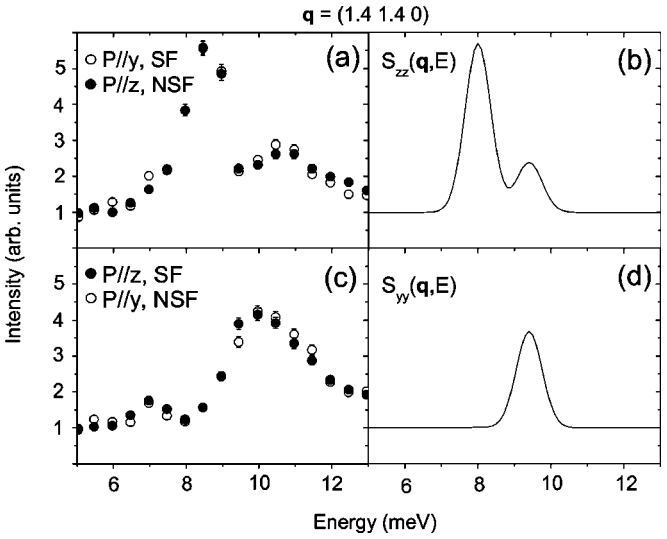

FIG. 12. Measured and calculated inelastic neutron scattering spectra at $\mathbf{Q}=(1.4\ 1.4\ 0)$ in the scattering geometry of Fig. 5. Panel (a) shows the fluctuations parallel to the z direction and panel (c) the fluctuations parallel to the y direction. The 8.5 meV peak in panel (a) corresponds to the acoustic branch, and the 10.5 meV peak to the two optical branches. The 7 meV peak is nonmagnetic in nature. The theoretical cross sections in panels (b) and (d) have been Gaussian broadened to match the experimental resolution. The single plotted curve in panels (b) and (d) should match both data sets in panels (a) and (c), respectively.

As for Fig. 10, the generalized susceptibility tensor rewritten in the suitable reference frame gives

$$\chi_{yy}=\chi_{zz}=\frac{\chi_{\bar{x}\bar{x}}+\chi_{\bar{y}\bar{y}}}{2}. \tag{9}$$

Of course, this experimental configuration cannot detect any anisotropic behavior in the magnetic fluctuations; this is confirmed by the present experimental result, as a spin-flip ratio 1/2 is detected for all branches.

On the other hand, returning to Fig. 5 but supposing the 3-$\mathbf{k}$ structure is longitudinal, the acoustic branch can be identified with $\omega^{\bar{z}\bar{z}}(\mathbf{Q})$ and the optical branch with $\omega^{\bar{x}\bar{x}}(\mathbf{Q})$ and $\omega^{\bar{y}\bar{y}}(\mathbf{Q})$; therefore, the y-y spin-flip fraction would be 0 for the former ($I_{zz}=0$) and 1 for the latter ($I_{yy}=0$). As this is not compatible with the experimental data, polarization analysis clearly discriminates between 3-$\mathbf{k}$ longitudinal and 3-$\mathbf{k}$ transverse excitations. Of course, this is more readily shown by the absence of the elastic (001) Bragg peak in the case of a longitudinal structure.

As far as all other investigated directions are concerned, the calculated polarizations well reproduce the measured ones whenever optical and acoustic branches are energetically well separated.

The above results do not depend on the precise values of the three parameters of the model (J,K,δ). The correct range for these values has been set by a qualitative matching of the model with the observed static properties and spin-wave frequencies. For all three parameters we obtain values close to those used in Ref. 16. In particular, a slightly larger value of

T_N (40 K) with respect to the experimental one had to be assumed in order to match spin-wave energies. No attempts were made to precisely fit the experimental dispersion curves, since the presence of three branches makes it difficult as only two branches are allowed by the present model. However, it was verified that the calculated spin-flip fractions are unchanged if the values of J and K are varied in the range consistent with macroscopic behavior. This is also true when different values of the anisotropic exchange ratio are used.

When acoustic and optical branches are well separated, the agreement between the theoretical and experimental spin-flip fractions is very good, and in particular the peculiar behavior of the acoustic mode is confirmed. Instead, for **Q** values where acoustic and optical branches are close in energy, the spin-flip fractions extracted from the experimental data appear to deviate from the calculated ones. These deviations are not understood at present. They might be due to effects not included in the present model (e.g., spin-phonon interactions, or whatever produces the third spin-wave branch). However, we cannot completely rule out that the deviations are an artefact, due to the difficulty of assigning the measured total scattering intensity to the different spin-wave modes, when their energies are closer than the experimental energy resolution. In fact, the deviation of the experimental ratios from the calculated ones resembles that expected for not fully discriminated spin-wave peaks.

V. CONCLUSIONS

The polarization of the spin-wave modes in the ordered 3-**k** state of UO_2 has been examined, experimentally and theoretically, using three-dimensional polarization analysis techniques. The information obtained allows the directions and relative amplitudes of fluctuations giving rise to the inelastic scattering event to be assessed. The measured polarizations of acoustic and optical branches of UO_2 are consistent with those expected for the 3-**k** static ordered structure, at least at points in reciprocal space where branches are well separated in energy. Exact quantitative calculations suffer from the well-known problems of calculating the exact dispersion relations, but the qualitative results obtained here are not strongly influenced by changes of the model parameters within physically reasonable limits. No direct evidence for magnon-phonon interactions was found.

An important issue in our calculations is that the observed polarization behavior emerges in a natural way under the assumption of 3-**k** order. Assuming a 1-**k** structure, a similar behavior can in principle be obtained, but only for anisotropic exchange parameters satisfying particular conditions. That is, whereas for a 3-**k** structure the observed anisotropic fluctuations occurs whatever the coupling strength, in a 1-**k** structure it could only be the result of an accident. This indicates that the behavior observed here is the generalization of the observations of Jensen and Bak[22] in the longitudinal 3-**k** material USb to all 3-**k** systems.

It would be interesting to perform similar measurements on other 3-**k**-ordering compounds, such as USb (Ref. 20) or NpBi.[21] These compounds order in a longitudinal structure, with well-defined spin waves whose dispersion and intensities are well reproduced by a model of localized 5f electrons in a crystal field.[17,22] Spin-wave polarization measurements could be used to test quite selectively the correctness of the theoretical picture for USb. Indeed, this picture has been put into question several times because the excited crystal-field states the model predicts were not experimentally observed.[23]

ACKNOWLEDGMENTS

The authors thank Paul du Plessis of the Witwatersrand University, South Africa, for the loan of the UO_2 crystal, and Tim Ziman, Stefano Carretta, and Giuseppe Amoretti for helpful discussions. One of the authors (E.B.) would like to thank the European Commission for support in the frame of the "Training and Mobility of Researchers" programme.

*Electronic address: elizabeth.blackburn@ill.fr

[1] P. J. Brown, J. B. Forsyth, and F. Tasset, Proc. R. Soc. London, Ser. A **442**, 147 (1993).
[2] F. Tasset, Physica B **297**, 1 (2001).
[3] P. J. Brown, J. B. Forsyth, and F. Tasset, J. Phys.: Condens. Matter **10**, 663 (1998), and references therein.
[4] J. A. Paixao, M. Ramos Silva, S. A. Sorensen, B. Lebech, G. H. Lander, P. J. Brown, S. Langridge, E. Talik, and A. P. Goncalves, Phys. Rev. B **61**, 6176 (2000).
[5] M. Blume, Phys. Rev. **130**, 1670 (1963).
[6] S. V. Maleyev, V. G. Bar'yakhtar, and R. A. Suris, Sov. Phys. Solid State **4**, 2533 (1963).
[7] L. P. Regnault, F. Tasset, J. E. Lorenzo, T. Roberts, G. Dhalenne, and A. Revcolevschi, Physica B **267–268**, 227 (1999).
[8] R. Caciuffo, G. Amoretti, P. Santini, G. H. Lander, J. Kulda, and P. de V. Du Plessis, Phys. Rev. B **59**, 13892 (1999).
[9] G. Amoretti, A. Blaise, R. Caciuffo, J. M. Fournier, M. T. Hutchings, R. Osborn, and A. D. Taylor, Phys. Rev. B **40**, 1856 (1989).
[10] D. Ippolito, L. Martinelli, and G. Bevilacqua, Phys. Rev. B **71**, 064419 (2005).
[11] J. Faber and G. H. Lander, Phys. Rev. B **14**, 1151 (1976).
[12] K. Ikushima, S. Tsutsui, Y. Haga, H. Yasuoka, R. E. Walstedt, N. M. Masaki, A. Nakamura, S. Nasu, and Y. Onuski, Phys. Rev. B **63**, 104404 (2001).
[13] S. B. Wilkins, R. Caciuffo, C. Detlefs, J. Rebizant, E. Colineau, F. Wastin, and G. H. Lander, cond-mat/0508394 (unpublished).
[14] R. A. Cowley and G. Dolling, Phys. Rev. **167**, 464 (1968).
[15] W. J. L. Buyers and T. M. Holden, in *Handbook of the Physics and Chemistry of the Actinides*, edited by A. J. Freeman and G. H. Lander (North-Holland, Amsterdam, 1985), Vol. II, p. 239.
[16] P. Giannozzi and P. Erdös, J. Magn. Magn. Mater. **67**, 75 (1987).
[17] B. Hälg and A. Furrer, Phys. Rev. B **34**, 6258 (1986).

[18] The relation between our parameters and those of Ref. 17 is $J=2J_0$, while we define $\delta=(J_1^l-J_1^t)/|J_1^t|$. The off-diagonal exchange parameter J_1^a has no effect on spin waves in the high-symmetry directions considered here.

[19] S. W. Lovesey, *Theory of Neutron Scattering from Condensed Matter* (Clarendon, Oxford, 1984).

[20] G. H. Lander and W. G. Stirling, Phys. Rev. B **21**, 436 (1980).

[21] F. Bourdarot, J. Bossy, P. Burlet, B. Fak, P. Monachesi, J. Rebizant, L. P. Regnault, J. C. Spirlet, and O. Vogt, Phys. Rev. B **56**, 14029 (1997).

[22] J. Jensen and P. Bak, Phys. Rev. B **23**, R6180 (1981).

[23] R. Osborn, M. Hagen, D. L. Jones, W. G. Stirling, G. H. Lander, K. Mattenberger, and O. Vogt, J. Magn. Magn. Mater., **76–77**, 429 (1988).